ARTICLES

Shape Selective Growth of CdS One-Dimensional Nanostructures by a Thermal Evaporation Process

Soumitra Kar* and Subhadra Chaudhuri*

Department of Materials Science, Indian Association for the Cultivation of Science, Kolkata 700 032, India

Received: October 22, 2005; In Final Form: January 9, 2006

CdS one-dimensional nanoforms such as nanowires, nanoribbons, networklike nanowires, pearl necklace type nanowires, helical-like nanowires, and nanowire arrays were formed on Si substrates by a simple thermal evaporation route. The shapes of the one-dimensional CdS nanoforms were controlled by varying the experimental parameters such as temperature and position of the substrates. Formation of the CdS one-dimensional nanoforms was initiated by the Au catalyzed vapor−liquid−solid technique, whereas the vapor−solid process played a crucial role in defining the shapes of the nanoforms. Different optical characterizations such as optical absorbance, photoluminescence, and Raman spectroscopy were adopted to explore the physical and structural quality of these CdS nanoforms.

1. Introduction

Single-crystalline, one-dimensional semiconductor nanostructures are considered to be one of the critical building blocks for nanoscale optoelectronics.[1−7] CdS is an important II−VI semiconducting material used for a host of applications in optoelectronics such as nonlinear optics, flat panel displays, light emitting diodes, lasers, and thin film transistors.[8−13] Recently, a thin film transistor was fabricated on CdS nanoribbons[8] and lasing was observed on individual CdS nanoribbons[9] and nanowires.[14] The preparation of nanocrystals with different morphologies provides an opportunity to explore the dependence of material properties on crystal structure, size, and shape. CdS nanowires were prepared by template assisted electrochemical routes,[15,16] the sol−gel technique,[17] the polymer assisted solvothermal process,[18] the vapor−solid (VS) method,[19] and metal catalyzed vapor−liquid−solid (VLS) techniques.[20,21] CdS nanobelts have been prepared by catalytic and noncatalytic thermal evaporation approaches.[8,9,22,23] However, these are all nonaligned CdS one-dimensional nanostructures. Synthesis of vertically aligned nanowire arrays is a critical step toward achieving the goal of nanoscale device fabrication.[24−26] Oriented CdS nanowires can be an ideal material for the applications in nanoscale devices. Thus, synthesis of aligned CdS nanowire arrays is an ongoing objective. Template assisted synthesis has been a common approach employed so far to fabricate aligned CdS nanowires.[15,17] However, the drawbacks of the template assisted approach is that, after the removal of the template, the embedded arrays of nanowires with a high aspect ratio normally collapse into an entangled mess due to the surface tension exerted on the nanowires during the evaporation of the liquids.[15,27] This makes the template assisted synthesis greatly limited when vertically aligned nanowire arrays are desired for applications in nanoscale devices.

In this work, we have prepared CdS one-dimensional nanostructures by a simple thermal evaporation route with different shapes such as nanowires, pearl necklace type nanowires, networklike nanowires, helical type nanowires, nanoribbons, and nanowire arrays. The synthesis temperature and the relative positions of the substrates with respect to the source were crucial factors in defining the shapes of the CdS nanostructures. To the best of our knowledge, we have prepared for the first time template free CdS nanowire arrays on Si wafers by a catalyst assisted thermal evaporation route. The optical properties of the CdS nanostructures were also studied to explore the physical properties of these CdS one-dimensional nanostructures.

2. Experimental Section

The details of the experimental setup have been described elsewhere.[28] In short, a conventional horizontal tube furnace was used for the synthesis. The Si wafers used, as the substrates, were first ultrasonically cleaned in acetone for 20 min. A thin (∼25 Å) layer of Au film was coated on the Si substrates by the sputtering technique. CdS powder, used as the precursor, was prepared through a chemical route by adding aqueous Na_2S solution dropwise to the aqueous solution of $Cd(NO_3)_2$ with vigorous stirring, and Ar gas was bubbled through the aqueous solution to prevent oxidation. An appropriate amount of the powder was loaded into a quartz boat. Then, the Si substrates were placed at different positions inside the quartz tube with respect to the quartz boat containing the CdS powder. The first Si substrate was clipped over the quartz boat with the Au coated surface facing the CdS powder in such a way that the vertical distance between the CdS powder and the Si substrate was ∼3 mm. The quartz boat was then placed near the closed end of a quartz tube. The other Si wafers were placed next to the quartz boat at distances of 1 and 6 cm from the boat with the Au coated

* To whom correspondence should be addressed. Phone: +91-033-2473-4971. Fax: +91-033-2473-2805. E-mail: kar_mitra@yahoo.co.in (S.K.); mssc2@iacs.res.in (S.C.).

10.1021/jp056058n CCC: $33.50 © 2006 American Chemical Society
Published on Web 02/18/2006

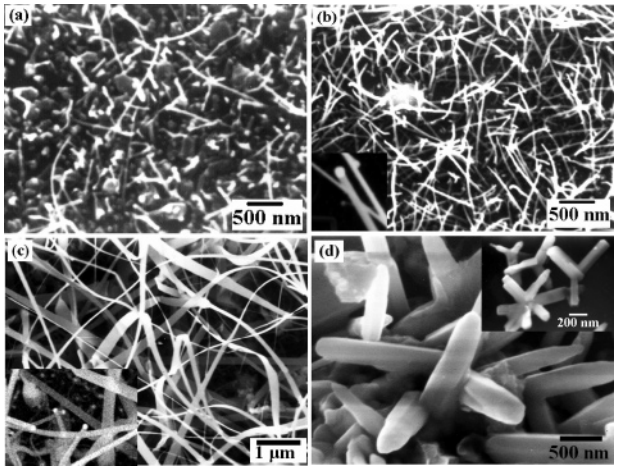

Figure 1. SEM image of the CdS nanostructures produced on the Si wafer placed directly over the source powder at different temperatures: (a) 800 °C; (b) 900 °C; (c) 950 °C; (d) 1000 °C. The insets in images b and c reveal the presence of Au nanoparticles at the tips of the nanowires and nanoribbons. The inset in part d shows multiarmed CdS nanorods.

surface on the up side. After evacuating the quartz tube up to 10^{-3} Torr, Ar gas was flown through it with a flow rate of 100 cm^3/min and was maintained for the entire deposition period. Subsequently, the quartz tube was inserted into a preheated tube furnace and taken out of it after 45 min of deposition to allow rapid cooling to room temperature. The deposition temperatures were 800, 900, 950, and 1000 °C for different sets of experiments.

The products were characterized using an X-ray diffractometer (Seifert 3000P) with Cu Kα radiation, and the compositional analysis was done by energy dispersive analysis of X-rays (EDAX, Kevex, Delta Class I). Microstructures of the nanoforms were studied by scanning electron microscopy (SEM, Hitachi S-2300) and transmission electron microscopy (TEM, JEM 2010). Photoluminescence (PL) measurements were carried out at room temperature with a luminescence spectrometer (Perkin-Elmer, LS50B) using 400 nm as the excitation wavelength. Raman spectra were recorded using a SPEX 1403 monochromator equipped with a direct current (dc) detection device. The 488 nm laser line of an Ar ion laser was used for excitation with an output power of 20 mW.

3. Results and Discussion

3.1. Microstructural Studies. For the microstructural studies, the as-deposited Si wafers were directly transferred to the SEM chamber without disturbing the original nature of the deposited yellow products on the Au coated surface. Figure 1 shows the SEM images of the products produced at different temperatures over the Si wafer placed directly over the quartz boat containing the CdS powder. Figure 1a shows the products obtained at 800 °C, which consisted of only a few nanowires. Figure 1b shows the formation of a large quantity of nanowires at 900 °C. The diameters of these nanowires were ∼50 nm and the lengths ∼1 μm. The image shown in the inset of Figure 1b reveals the presence of the Au nanoparticles at the tip of the nanowires. The composition of the particles was confirmed from EDAX studies, which will be discussed later. Further increase of temperature to 950 °C produced a large number of nanoribbons (Figure 1c), having widths ranging from 200 to 250 nm and lengths of the order of a few micrometers. The Au nanoparticles were also detected at the tip of the CdS nanoribbons, as can be seen in the SEM image shown in the inset of Figure 1c. At a

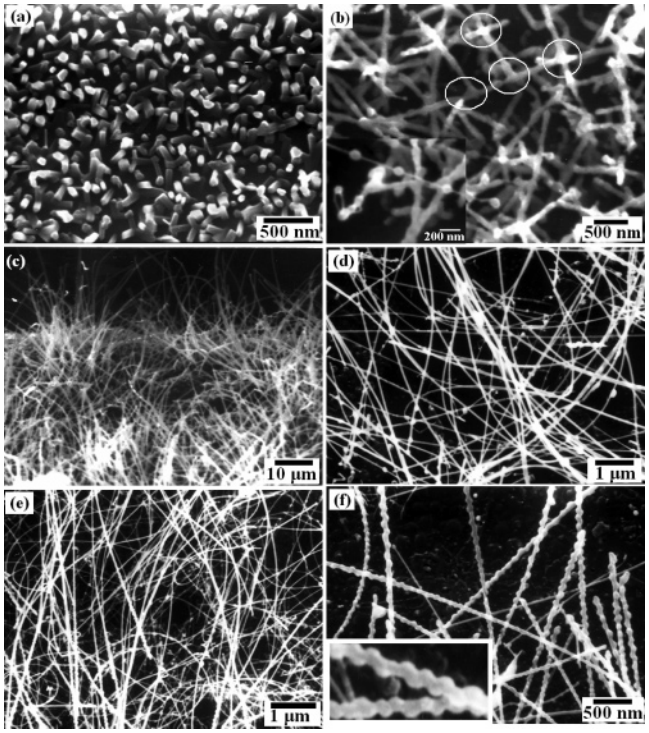

Figure 2. SEM images of the CdS nanowires produced at different substrate positions toward the downstream side and at different temperatures: (a) 6 cm away from the source at 900 °C; (b) 6 cm away from the source at 1000 °C; (c and d) 1 cm away from the source at 950 °C; (e and f) 1 cm away from the source at 1000 °C. A magnified SEM image of a helical-like wire is shown in the inset of part f.

temperature of 1000 °C, thick nanorods with diameters of 200−400 nm and lengths of ∼2 μm were observed (Figure 1d). Along with these nanorods, a few multiarmed nanostructures were also produced, as displayed in the inset of Figure 1d. Thus, from the SEM observations, it was indicated that an increase in the synthesis temperature increases the dimensionality of the CdS nanostructures. Lower temperatures favor the formation of CdS nanowires, whereas nanoribbons are formed at relatively high temperatures. However, excessively high temperatures favor the formation of submicrometer column structures.

Many interesting 1-D nanostructures were formed on the Si substrates placed toward the down stream edge, as can be seen from the SEM images in Figure 2. The SEM images in parts a and b of Figure 2 show the products obtained on the Si substrates at a distance of 6 cm from the source powder at temperatures of 900 and 1000 °C, respectively. Figure 2a shows that short column structures were formed perpendicular to the surface of the substrates. Figure 2b reveals the formation of networklike CdS nanowires. A few junction points of the branched network structures were highlighted in the figure by drawing circles around them.

Along with these networklike nanowires, a few pearl necklace type nanowires were also detected, as revealed by the inset of Figure 2b. The SEM image in the inset of Figure 2b reveals the presence of spherical nanoparticles in the nanowires at regular intervals, giving it the precise look of a necklace. Figure 2c and d reveals the formation of ultralong uniform nanowires on the Si substrates placed next to the CdS powder source at 950 °C. These nanowires have diameters within 40−60 nm and lengths of ∼50 μm. When the temperature was increased to 1000 °C, CdS nanowires were still observed (Figure 2e and f) at the same position, that is, over the substrates next to the source. However, the diameters of the nanowires were slightly

increased, varying within 50−100 nm. Magnified SEM images revealed the presence of a few helical-like nanowires, as can be seen in Figure 2f. These nanowires might not be exactly of the helical type, but they were quite close to it, as can be seen in the inset of Figure 2f.

All of these CdS nanoforms were nonaligned with some degree of orientation being observed on the sample obtained at a distance of 6 cm at 900 °C. The results discussed above indicated that, at the same temperature, say 950 °C, CdS nanoribbons were observed when the substrate was directly clipped over the source while CdS nanowires were obtained when the substrate was placed next to the quartz boat containing CdS powders. The temperature was the same for both positions of the substrates. These results indicated that low but steady vapor concentrations of the CdS favor the formation of nanowires. Thus, the basic requirement for obtaining the desired nanowire arrays was to ensure slow but steady flow of the CdS molecular vapors perpendicular to the Au coated Si substrate for a brief period of time. For this purpose, a quartz container of the CdS source powder, which served the dual purpose of the substrate holder as well as the container for the source CdS powder, was specially designed. The quartz boat was centrally covered with two open horizontal channels on both sides of it. The boat was filled with CdS powder, and the Au coated Si wafer was placed on one of the open channels with the Au layer facing the CdS powder from a distance of ∼3 mm. Almost the total area of one of the open channels was covered by the wafer, keeping two narrow slitlike openings on both sides of it for the exit of the carrier Ar gas from the quartz boat. The carrier Ar gas entered through the other opening at high temperature and carried the CdS molecular vapors to the side having the Si wafer where it struck the wafer steadily before coming out of the boat through the small openings on both sides of the Si wafer. Figure 3a and b shows the SEM image of the products after 45 min of deposition, revealing the formation of well-aligned CdS nanowire arrays. A cross-sectional view of the nanowire arrays is shown in the inset of Figure 3b. This image indicates the presence of spherical particles at the tips of the nanowires. All of the nanowires were almost identical in length and diameter, which is important for the fabrication of devices. The diameters of the nanowires were about 60 nm, and the lengths were ∼1 μm. The SEM images also indicate the cross sections of the nanowires to be circular. For the purpose of understanding the growth mechanism, the experiment was performed for 15 min and the resultant products are shown in Figure 3c. On the basis of these results and further investigation of TEM images, the growth mechanism of the CdS nanoforms will be discussed in the following section.

3.2. Structural and Chemical Compositional Analysis. The crystal structure of the products was confirmed by the X-ray diffraction (XRD) patterns. The XRD patterns of all of the samples except the nanowire arrays were almost identical in nature, and one representative pattern is shown in Figure 4a. All of the peaks corresponding to the hexagonal wurtzite phase of CdS with lattice constants of $a = 4.14$ Å and $c = 6.72$ Å match well with those in the JCPDS data (Joint Committee on Powder Diffraction Standards, card no. 41-1049). The XRD pattern of the CdS nanowire arrays is shown in Figure 4b, revealing the formation of wurtzite CdS along with the presence of two tiny peaks at $2\theta = 38.18$ and 44.38° due to Au (JCPDS card no. 04-0784). The compositions of the nanostructures were further studied from the energy dispersive analysis of X-rays (EDAX). The EDAX spectrum recorded over the nonaligned CdS 1-D nanoforms revealed the presence of only Cd and S in a near stoichiometric ratio (Cd/S = 51.4:48.6), whereas the EDAX spectrum recorded over a selected area of the nanowire arrays indicates the presence of Au along with the presence of Cd and S, which is shown in Figure 4c. However, the EDAX spectrum recorded separately on the stem of these nanowires revealed the presence of only Cd and S in a near stoichiometric ratio (Cd/S = 51:49). On the other hand, the spectrum recorded on the spherical particle present at the tip area of the nanowires and nanoribbons indicated the presence of Au in an appreciable amount. Thus, the EDAX spectra indicated the presence of different materials at the tips of the nanowires, that is, the Au nanoparticles.

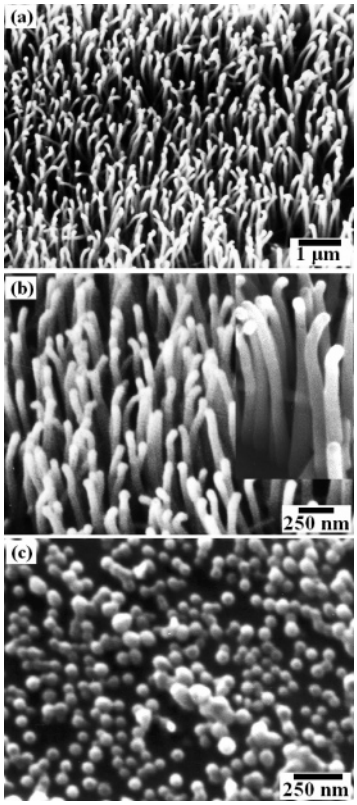

Figure 3. SEM image of the CdS nanowire arrays deposited at 900 °C: (a) low magnification image; (b) high magnification image. A cross-sectional view of the CdS nanowire arrays is shown in the inset of part b. The image in part c reveals the initial stage of the CdS nanowire array formation.

3.3. TEM Studies. The morphology and crystal structure of the CdS nanostructures were further confirmed from the transmission electron microscopy (TEM). Figure 5a shows the TEM images of the CdS nanowires produced at 950 °C, while the TEM image of a single nanoribbon is shown in Figure 5b. The ripplelike contrasts observed on the CdS nanowires and nanoribbons are due to the strains caused by the bending of the nanoforms. Parts c and d of Figure 5 show the base and tip area of a CdS nanowire, which was collected from the CdS nanowire arrays. The presence of a spherical Au nanoparticle at the tip of the CdS nanowire was confirmed from Figure 5d. One representative high resolution transmission electron microscopy (HRTEM) image of a single CdS nanowire is shown in Figure 5e, and the corresponding selected area electron diffraction (SAED) pattern is shown in the inset. Both of the patterns reveal that these CdS nanowires were perfectly single crystalline, having a hexagonal wurtzite structure. The measured spacing of the lattice fringes in the HRTEM image was 3.36 Å, which corresponds to the (002) plane of the wurtzite CdS. This (002) direction was also the growth direction of the CdS

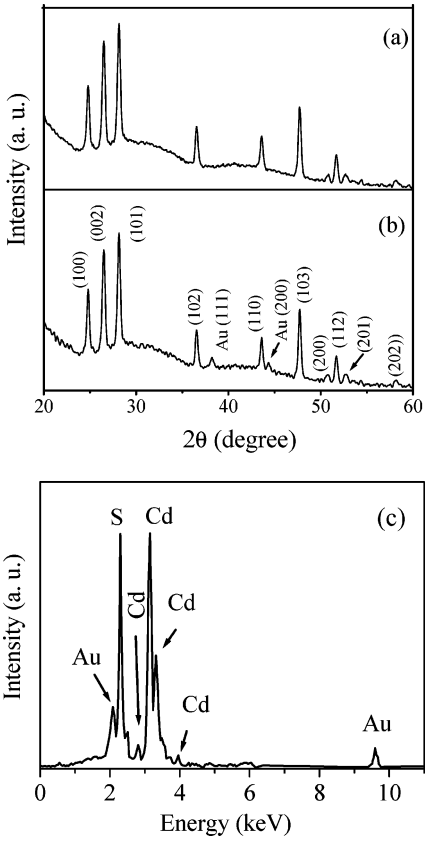

Figure 4. XRD patterns of the CdS (a) nonaligned nanowires and (b) aligned nanowire arrays. (c) EDAX spectrum of the CdS nanowire arrays.

nanowires, and this was also confirmed from the SAED pattern. The (100) lattice plane corresponding to the hexagonal wurtzite CdS is also indicated in the SAED pattern. Figure 5f shows the TEM image of the sample corresponding to the SEM image shown in Figure 3c. This image reveals the presence of a few dark contrast particles along with a light contrast elongated structure. The EDAX measurement facility available with the TEM indicated that the dark nanoparticles mainly consisted of Au whereas the elongated light portions were pure CdS. These two SEM (Figure 3c) and TEM (Figure 5f) images showed the initial nucleation stage of the nanowires from the Au nanoparticles.

3.4. Growth Mechanism. Two well established routes for the growth of nanowires and nanoribbons are the catalyst assisted vapor−liquid−solid (VLS)[29,30] and vapor−solid (VS)[31−33] methods. In the VLS process, a thin layer of metal catalyst such as Au is deposited on the substrate, which at high temperature breaks up to form liquid nanodroplets. These metal droplets absorb the incoming source of molecular vapor, and finally, upon supersaturation, solid nanostructures start appearing with the metal nanoparticles at their tips. Thus, the key characteristic of the VLS growth process is the existence of the metal nanoparticles at the tips of the nanostructures. On the other hand, in the VS method, the source materials vaporize to the molecular level with stoichiometric cation−anion molecules which condense to the substrate and the molecules are arranged in such a way that the proper local charge balance and the structural symmetry are maintained, resulting in a nucleation center. With further intake of the molecules, the surfaces that have lower energy, for example, side surfaces, start to form and the low energy surfaces tend to be flat. In our case, we believe that for the uniform nanowires and the nanowire arrays the VLS process was the main growth mechanism whereas for the CdS nanoribbons and other types of nanowires, namely, networklike, pearl-necklace-like, and helical-like nanowires, the VLS and VS processes are equally responsible for the evolution of the typical morphologies. On the basis of our SEM and TEM observations and the existing growth models, we explain the formation of different 1-D CdS nanoforms, and for simplicity, the growth mechanism is presented with a schematic diagram shown in Figure 6. The rectangular cross section of the CdS nanoribbons suggests that the conventional VLS process alone cannot be the growth mechanism. Thus, at high CdS vapor concentrations, the CdS vapor species were not only absorbed by the Au liquid droplets but also deposited below the Au nanodroplets which were still in their restructuring stage, that is, in the high energy state. As a result, the widths of the nanostructures increased and by the influence of the VS method CdS nanoribbons originated. Since the growth of CdS nanoribbons is initiated by the Au catalyst nanoparticles via the VLS process, the sizes

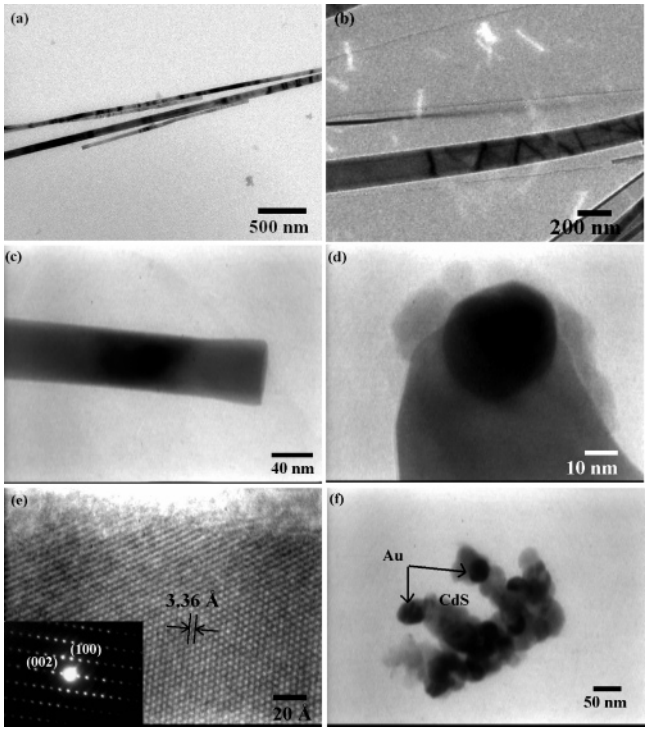

Figure 5. TEM images of the CdS nanoforms: (a) CdS nanowires produced at 950 °C over the substrates placed 1 cm away from the source; (b) CdS nanoribbon; (c) base region of a CdS nanowire from the nanowire array sample; (d) tip of the above nanowire revealing the presence of a Au nanoparticle at its tip; (e) HRTEM image of a single CdS nanowire along with the corresponding SAED pattern in the inset; (f) TEM image showing the initial nucleation stage of the CdS nanowires.

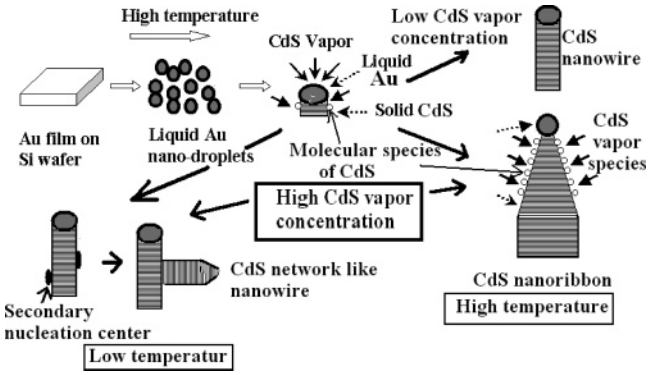

Figure 6. Schematic view of the formation of different CdS nanoforms.

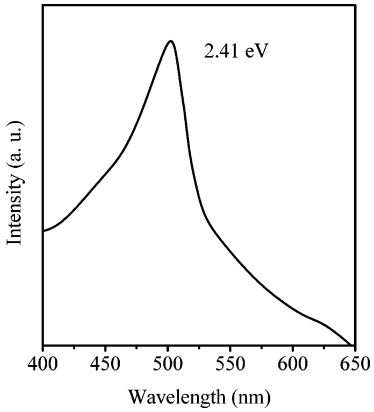

Figure 7. Room temperature optical absorption spectrum of the CdS nanowires.

of the Au nanoparticles may be useful to control the thicknesses of the CdS nanoribbons. Thus, at the lowest possible temperature favoring the CdS nanowire formation, that is, at 900 °C, the slow but steady supply of the CdS vapors surrounding the Au liquid nanodroplets ensures the formation of the nanowires perpendicular to the substrates. For the fabrication of CdS nanowire arrays, the role of the quartz boat containing the CdS powder was most crucial. In the same experimental arrangement when the topside open boat was used as the source container and the substrate holder, nonaligned nanowires were formed, whereas with the specially designed container aligned nanowire arrays were formed. The formation of the networklike and pearl-necklace-like nanowires (Figure 2b) at a distance of 6 cm from the source at 1000 °C could also be due to the influence of the VS process. In this case, the temperature of the substrate region was ~850 °C. The nanowires were initially formed by the VLS technique. At the high temperature, the CdS powder sublimes quickly, and as a result, the CdS vapor concentration surrounding the substrates was also high. The nanowire formation was initiated by the Au catalyzed VLS technique. However, as the temperature was relatively low, the mobility of the newly arrived molecules was also low; as a result, those CdS species deposited on the side wall of the nanowires could not move to the growth front and instead remained on the wall of the nanowires, giving rise to the nonuniform diameter of the nanowires. This might result in some rough patch or kink on the nanowire surface which acts as the energetically favored site for the newly arrived vapor species to be absorbed on it, giving rise to the branched or networklike structures. The pearl necklace formation could be explained by the fact that when the diameter of the Au particle was small, the growth due to the VLS process was fast, but due to the lower mobility, the molecules absorbed on the surface could not move rapidly; that is, they were lagging behind the Au mediated growth, resulting in the formation of flattening or pearl-like structure formation at regular intervals. The helical-like structure formation as shown in Figure 2e and f could be due the same reason that was discussed above.

3.5. Optical Absorption Studies. For the optical absorption study, the nanoforms were scratched from the surfaces of the substrates and subsequently dispersed ultrasonically in ethanol. The optical absorption spectra for the CdS nanowires and nanoribbons were quite similar to each other. Figure 7 shows the optical absorption spectra of the CdS nanowires. The figure shows sharp excitonic nature of the optical absorption spectrum. The band edge was determined from the peak position of the first derivative of the absorption spectrum at 514 nm, that is, at 2.41 eV. This was the bulk band gap of CdS. Thus, the optical absorption study reveals an excellent crystal quality of the CdS nanostructures.

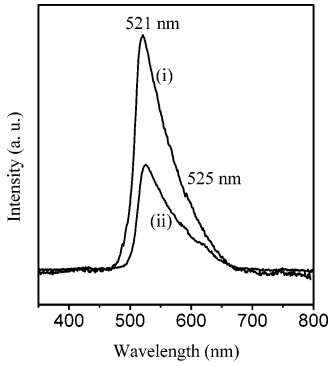

Figure 8. Room temperature PL spectra of the (i) CdS nanowire arrays and (ii) nonaligned CdS nanowires.

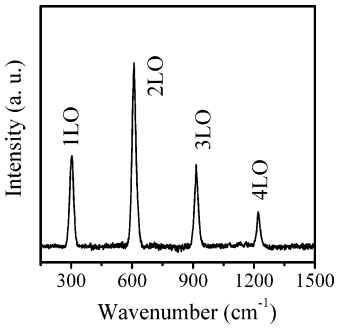

Figure 9. Raman spectra of one representative CdS nanowire sample.

3.6. Photoluminescence Properties. The photoluminescence (PL) properties of the CdS nanostructures were measured at room temperature with a view to further assess their quality. Figure 8 shows the room temperature PL spectra recorded with 400 nm excitation. Although from all of the CdS nanostructures intense green emission was observed, maximum intensity was observed for the CdS nanowire arrays. The intensities were almost identical for the CdS nanowires and nanoribbons. The peak position of the green emission for the nanowire arrays was at ~521 nm, and for the other structures, this was at 525 nm. This peak corresponds to the near band edge emission. Similar band edge emission was also reported on CdS nanoribbons.[9] Red emission was also reported due to the trapped luminescence from CdS nanowires.[20] The absence of the emissions from the surface and deep states associated with the defects and impurities demonstrate that these single-crystal CdS nanowire arrays possess high quality optical properties and should be excellent building blocks for photonic devices.

3.7. Raman Studies. Raman spectroscopy is a powerful tool for the investigation of the doping concentration, lattice defect identification, and crystal orientation properties of the materials. The Raman spectra for all of the CdS nanostructures were more or less identical, and one such representative spectrum is shown in Figure 9. The Raman peaks were analogous to the pure crystalline CdS.[34,35] The peaks at 305, 609, 915, and 1215 cm^{-1} correspond to the first-order (1-LO), second-order (2-LO), third-order (3-LO), and fourth-order (4-LO) longitudinal optical phonon bands of CdS, respectively.

4. Conclusions

We have fabricated CdS one-dimensional nanostructures with different interesting shapes. Morphological control of the CdS

products was achieved by changing the experimental parameters, such as temperature and position of the substrates. We have for the first time fabricated CdS nanowire arrays on Si substrates by a template free VLS process. It is proposed that the growth of the CdS one-dimensional nanoforms was initiated by the Au mediated VLS technique, whereas, occasionally, the shapes of these nanoforms were controlled by the VS method. Optical characterizations of the products reveal their good optical as well as excellent crystalline qualities. CdS nanowire arrays could be an ideal building block for the fabrication of nanoscale optoelectronic devices.

References and Notes

(1) Xia, Y.; Yang, P.; Sun, Y.; Wu, Y.; Mayers, B.; Gates, B.; Yin, Y.; Kim, F.; Yan, H. *Adv. Mater.* **2003**, *15*, 353.
(2) Han, W. Q.; Fan, S. S.; Li, Q. Q.; Hu, Y. D. *Science* **1997**, *277*, 1287.
(3) Morales, A. M.; Lieber, C. M. *Science* **1998**, *279*, 208.
(4) Lieber, C. M. *Solid State Commun.* **1998**, *107*, 607.
(5) Heath, J. R.; Kuekes, P. J.; Snyder, G. S.; Williams, R. S. *Science* **1998**, *280*, 1716.
(6) Hu, J.; Ouyang, M.; Yang, P.; Lieber, C. M. *Nature* **1999**, *399*, 48.
(7) Wada, Y.; Yin, H.; Kitamura, T.; Yanagida, S. *Chem. Commun.* **1998**, *24*, 2683.
(8) Duan, X. Niu, C.; Sahi, V.; Chen, J.; Parce, J. W.; Empedocles, S.; Goldman, J. L. *Nature* **2003**, *425*, 274.
(9) Liu, Y. K.; Zapien, J. A.; Geng, C. Y.; Shan, Y. Y.; Lee, C. S.; Lee, S. T. *Appl. Phys. Lett.* **2004**, *85*, 3241.
(10) Zhang, J.; Jiang, F.; Zhang, L. *J. Phys. Chem. B* **2004**, *108*, 7002.
(11) Agata, M.; Kurase, H.; Hayashi, S.; Yamamoto, K. *Solid State Commun.* **1990**, *76*, 1061.
(12) Ullrich, B.; Bagnall, D. M.; Sakai, H.; Segawa, Y. *Solid State Commun.* **1999**, *109*, 757.
(13) Artemyev, M. V.; Sperling, V.; Woggon, U. *J. Appl. Phys.* **1997**, *81*, 6975.
(14) Agarwal, R.; Barrelet, C. J.; Lieber, C. M. *Nano Lett.* **2005**, *5*, 917.
(15) Xu, D.; Xu, Y.; Chen, D.; Guo, G.; Gui, L.; Tang, Y. *Adv. Mater.* **2000**, *12*, 520.
(16) Liang, Y.; Zhen, C.; Zou, D.; Xu, D. *J. Am. Chem. Soc.* **2004**, *126*, 16338.
(17) Cao, H.; Xu, Y.; Hong, J.; Liu, H.; Yin, G.; Li, B.; Tie, C.; Xu, Z. *Adv. Mater.* **2001**, *13*, 1393.
(18) Zhan, J.; Yang, X.; Wang, D.; Li, S.; Xie, Y.; Xia, Y.; Qian, Y. *Adv. Mater.* **2000**, *12*, 1348.
(19) Ye, C.; Meng, G.; Wang, Y.; Jiang, Z.; Zhang, L. *J. Phys. Chem. B* **2002**, *106*, 10338.
(20) Wang, Y.; Meng, G.; Zhang, L.; Liang, C.; Zhang, J. *Chem. Mater.* **2002**, *14*, 1773.
(21) Barrelet, C. J.; Wu, Y.; Bell, D. C.; Lieber, C. M. *J. Am. Chem. Soc.* **2003**, *125*, 11498.
(22) Dong, L.; Jiao, J.; Coulter, M.; Love, L. *Chem. Phys. Lett.* **2003**, *376*, 653.
(23) Kar, S.; Satpati, B.; Satyam, P. V.; Chaudhuri, S. *J. Phys. Chem. B* **2005**, *109*, 19134.
(24) Whang, D.; Jin, S.; Wu, Y.; Lieber, C. M. *Nano Lett.* **2003**, *3*, 1255.
(25) Huang, M. H.; Mao, S.; Feick, H.; Yan, H.; Wu, Y.; Kind, H.; Weber, E.; Russo, R.; Yang, P. *Science* **2001**, *292*, 1897.
(26) Wang, X.; Summers, C. J.; Wang, Z. L. *Nano Lett.* **2003**, *3*, 1315.
(27) Barbic, M.; Mock, J.; Smith, D. R.; Schultz, S. *J. Appl. Phys.* **2002**, *91*, 9341.
(28) Kar, S.; Chaudhuri, S. *J. Phys. Chem. B* **2005**, *109*, 3298.
(29) Wagner, R. S.; Ellis, W. C. *Appl. Phys. Lett.* **1964**, *4*, 89.
(30) Wu, Y.; Yang, P. J. *J. Am. Chem. Soc.* **2001**, *123*, 3165.
(31) Sears, G. W. *Acta Metall.* **1955**, *3*, 361.
(32) Yang, P.; Lieber, C. M. *J. Mater. Res.* **1997**, *12*, 2981.
(33) Pan, Z. W.; Dai, Z. R.; Wang, Z. L. *Science* **2001**, *291*, 1947.
(34) Leite, R. C. C.; Porto, S. P. S. *Phys. Rev. Lett.* **1966**, *17*, 10.
(35) Suh, J. S.; Lee, J. S. *Chem. Phys. Lett.* **1997**, *281*, 384.